This is a peer-reviewed, author's accepted manuscript of the following conference output:
Jones, C. E., Johny, J., Norman, P., & Burt, G. (2022).
At scale, experimental capture of electrical response of carbon fibre composites to inform integrated electrical power and structural systems.
Paper presented at Towards Sustainable Aviation Summit 2022, 3AF, Toulouse, France.

# At Scale, Experimental Capture of Electrical Response of Carbon Fibre Composites to Inform Integrated Electrical Power and Structural Systems.

Catherine. E. Jones, Jeffy Johny, Patrick Norman, Graeme Burt
University of Strathclyde, Glasgow, UK
catherine.e.jones@strath.ac.uk

*Abstract*- **The electrification of aircraft systems and the light weighting of aero-structures using carbon fibre reinforced polymers (CFRP) are two key enabling technologies supoorting the decarbonisation of flight. Close physical integration of the electrical and structural systems offers an opportunity to optimise the combined system weight and volume, and optimise system performance.**

**In such integrated structural systems, electrical current may flow through the CFRP under faulted conditions to reach the current return network. A major barrier to their design is the poorly understood low frequency (<MHz) electrical response of CFRP. This paper presents the extrapolation of the response of CFRP to higher currents, including investigation of power dissipation levels and the time taken to reach key threshold temperatures linked to the thermal degradation of CFRP. These results inform design criteria for integrated systems and dual use materials to enable the adaption of CFRP to handle return currents.**

## I. INTRODUCTION

Electrification of on-board aircraft systems is critical to improved overall aircraft efficiency for reduced fuel burn and greenhouse gas emissions [1]. A parallel underpinning technology for aircraft decarbonisation is the design and implementation of lightweight, carbon fibre reinforced polymer (CFRP) structures. More than 50% of the structure of a state of the art aircraft is constructed from CFRP, reducing structural weight by ~ 20% [2]. However, the poor electrical conductivity of CFRP results in industry standards requiring that electrical and CFRP structural systems are kept physically separate, e.g. [3], and that the CFRP structure cannot form the current return network. For aircraft with predominantly CFRP structures, the current return network is provided by a combination of existing metallic structures and additional cables where necessary [4].

The additional infrastructure for physical separation between electrical and structural systems adds weight and volume to the overall aircraft system, reducing the benefits of electrification and lightweight CFRP structures. For example, the additional infrastructure required for physical separation is estimated to contribute an additional 30% to the cabling weight on the aircraft [4].

A major challenge for the electrification of on-board systems, and in particular electrical propulsion systems, is the associated weight and volume of the electrical power system [6]. The target power densities and associated timelines for enabling technologes, including power electronics and electrical machines, are extremely challenging. Developing design methods for modularised, integrated electrical and structural systems which minimise the need for infrastructure to keep the electrical and CFRP structural systems separate, offers a route to reduce the weight and volume of one part of the system, and thereby reduce the power density required for another part of the system. Development of integrated systems for the electrical wiring interconnection system (EWIS) provides a platform for the design of modular sections of EPS equipment encased in CFRP, and the design of systems where the CFRP structure has combined electrical, strurctural and thermal capability [7].

In order to design these integrated electrical power and CFRP structural systems, it is necessary to understand the electrical properties and response of CFRP. To enable this, an electrical model of the pathway taken by electrical current as it is conducted through the CFRP is needed. This firstly enables studies to understand how the electrical power system and the CFRP will influence each other, for example, during an electrical fault [8,9]. Secondly, combining this knowledge with information regarding the thermal response of CFRP due to electrical conduction (caused by localised Joule heating) enables capture of design parameters regarding limits and thresholds for electrical current conduction before thermal degradation may occur. If the resin matrix is heated above its glass transition temperature, the mechanical strength of the CFRP is likely to be degraded. Hence capture of the electrical response of CFRP enables the capture of design criteria, both for the electrical power system (*e.g.* choice of grounding topology, fault management strategy and resulting choices of architecture and equipment topologies) and for the CFRP component design. This includes the method for electrically bonding a CFRP panel to ground to influence the pathway taken by electrical fault current to reach ground.

While previous studies have developed lumped impedance models for CFRP, and have investigated the electrical and thermal response of CFRP, the samples used have been relatively small in length and width (100 mm x 100 m x 5 mm) compared to actual aircraft components [8], and have been limited to 90 W power dissipation through a CFRP panel. This paper extends previously published models to larger panels of CFRP, and captures the thermal response at higher power levels (up to 250 W).

The rest of this paper is organised as follows: Section II describes in detail the challenges for integrating CFRP with an

electrical power systems on an aircraft, and as a result what the key information required from an electrical model of CFRP is; Section III describes the hypothesis for the revised lumped resistance electrical model, the experimental methods to capture parameters for this model and the resulting models developed; Section IV presents the captured relationships between power dissipation and time; Section V discusses the implications of these results for the design of integrated electrical power and CFRP structural systems, and conclusions and future work are given in Section VI.

## II. Challenges for integrated systems on Aircraft

### a. *Electrical and thermal properties of CFRP*

From an electrical perspective, CFRP is a highly complex material. CFRP is a hetergenous material, which consists of layers (plies) of carbon fibres, which are electrical conductors, held in a polymer resin, which is an electrical insulator. Aerospace grade CFRP has a volume fraction for carbon fibre of ~ 55 – 60%. The carbon fibres may be woven together in each ply, or fibres are arranged to lie parallel to each other, unidirectional (UD) CFRP. The orientation of fibres relative to other plies is varied to give a structure mechanical strength. The wavy nature of carbon fibres results in electrical connections between carbon fibres both within a ply and between adjacent plies. Hence electrical conductivity can be highly anisotropic, and is affected by several factors including choice of fibre, orientation and layup of the fibres, and the volume fraction of fibre [10]. The focus of this paper is pre-preg UD [0º] CFRP, with T800H polyacrylonitrile (PAN) carbon fibre [11] with HTC400 epoxy resin [12], with 54% volume fraction of carbon fibre. In UD [0º] layups, all carbon fibres are aligned in one direction, which provides a starting point for the development of electrical models.

Due to localised Joule heating, localised heating will occur along the pathway taken by electrical current through CFRP. Similar to electrical properties, there is a strong interdependency between layup and thermal properties due to the high thermal conductivity of carbon fibre compared to polymer resin [13]. Localised heating will occur at the interface between carbon fibres and the resin [14]. If the glass transition temperature, $T_g$, of the resin is reached, then the resin will start to degrade. However degradation may start to occur before this temperature is reached, due to localised heating between fibres and resin at the microscale. For the design of integrated systems, the correlation of power dissipation, temperature reached and time to reach that temperature, are all critical parameters to avoid thermal degradation of the structure in the integrated system. However, to estimate the power dissipation, the electrical pathway taken by electrical current through CFRP and the associated electrical impedance must be known.

To date low frequency (<MHz) electrical characterisation of CFRP has received limited attention in the literature. Methods to develop component scale electrical models based on numerical methods using variables at a microscale are presented, e.g. [15]. The waviness of fibres, and variation of volume fraction of carbon fibre in the material (at the microscale), result in non-uniform distribution of contact points between fibres. Hence such models are complex and computationally intensive. In order to integrate the electrical model of CFRP into a behavioural or functional simulation model of an electrical power system (or sub-system), the electrical model of the CFRP must be modelled at computational complexity compatible with these modelling approaches. For example, with CFRP as a lumped impedance, e.g. [16], these characteristics are captured at the macroscale from the outset rather than extrapolated from microscale values. While this is presented in [8], a limitation of this model is that it is only validated for a small (100 mm x 100 mm) square of UD [0º] CFRP.

### b. *Key considerations for integrated systems on aircraft*

State of the art more electric aircraft typically have a dual channel electrical power system, rated up to ~ 1.5 MW [1]. The aircraft electrical power system operates in a hazardous environment, with vibration the main cause of electrical faults [17]. Therefore a significant consideration for the design of an integrated electrical power and structural system is the influence that CFRP would have if it formed part of the pathway for fault current to reach the current return network.

A TN-C-S grounding topoology is implemented [18]. The approach to fault management for rail to ground faults for such a grounding topology is based on electrical faults with low resistance (< 0.01 Ω) resulting in high fault currents and undervoltages, and enabling a high level of selectivity for the isolation of these faults. The current return for the electrcal power system must be as close to an equipotential voltage as possible [3,19]. Therefore on aircraft which are predominatly made from CFRP structures, the current return is constructed from metallic structures with addition cables where necessary. The maximum electrical resistance for connections to the grounding and bonding network is 2.5 mΩ [3]. To prevent failure from a single fault, common ground connections are avoided. AC and DC grounds are kept separate.

While it is outwith the scope of this paper to consider it in detail, consideration must also be given to where electrical faults are likely to occur, the fault manifestation process, the type of electrical fault, and expected implications and severity if no action is taken. This paper seeks to contribute to answers to the final part of this question on the impact of electrical current on CFRP. If the relationships between electrical pathways taken through CFRP, the layup of the CFRP, the size and location of electrical bonds to ground, and the localised heating of the CFRP are characterised, then informed decisions on the design of these integrated systems can be made.

## III. Electrical model of UD [0°] at Scale

### a. *Modelling hypothesis*

A low (<1A) electrical current was injected through a silver epoxy electrode which is 10 mm x 10 mm on the surface of a

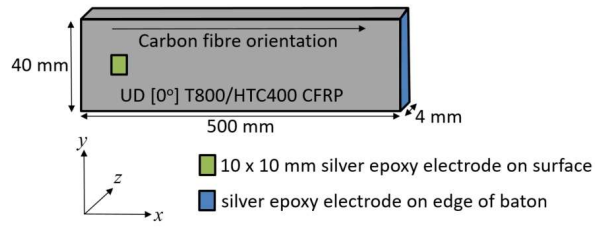


**Fig. 1: T800/HTC 400 CFRP sample with indication of location of electrodes.**

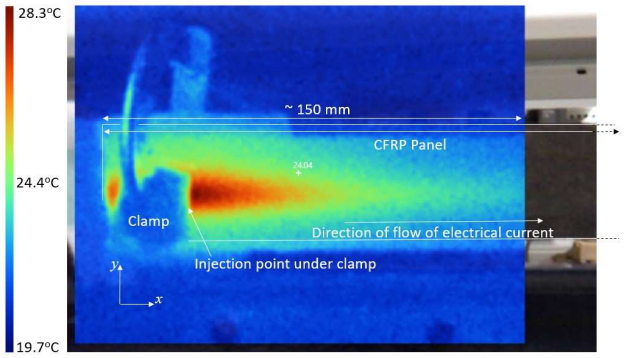


**Fig. 2: Thermal image of localised heating during conduction of current through CFRP baton.**

500 x 40 x 4 mm baton of T500/HTC400 CFRP and exited through a silver epoxy electrode on the edge of the CFRP, as indicated in Fig. 1. The surface electrode was prepared by sanding the injection area with 320 grit sandpaper, to remove the outer layer of epoxy. Copper foil electrodes were clamped to the CFRP using a vice to minimise contact resistance and establish a good electrical connection, as described in [16]. A thermal image of the section of the CFRP baton where the electrical current is injected is shown in Fig. 2. By inspection, it is clear that there is a concentration of heat dissipation at the entry point. Beyond the entry point, the temperature drops, indicating lower levels of power dissipation.

The electrical resitance, *R(Ω),* of a pathway through a material conducting electrical current with an electrical conductivity conductivity, σ (S/m) along a length, *l (m),* and cross-sectional conducting area, *A* ($m^2$), is given by

$$R = \frac{l}{\sigma A} \qquad (1).$$

With reference to the scenario shown in Fig. 2, by Kirchoff's law, as there is only one entry and exit point for the current being conducted by the CFRP, the current injected is the same as the current exiting the CFRP. The power, *P(W)*, dissipated by a resistor is given by

$$P = I^2 R \qquad (2),$$

where *I (A)* is the current conducted through the resistance, *R (Ω),* estimated from (1). Power is dissipated as heat. Hence if more heat is dissipated at one point in the conducting pathway than another, this indicates a higher resistance at that point. Combining this with the thermal image in Fig. 2, it is inferred that the electrical resistance of the pathway taken by the electrical current through the CFRP varies with location.

From the literature [9,10,16] the electrical conductivity of UD [0°] CFRP in the in-fibre ($x$) direction, is ~ 3 - 4 * $10^4$ S/m, in the cross-ply ($y$) direction it is ~$10^2$ S/m, and ~ 1 S/m in the through-thickness ($z$) direction. In previous models described in the literature, the resistance for the conducting pathway in the x-direction, has been modelled as a single resistance, taking the distance, *l,* as being from the edge of the electrode to the edge of the sample. However, these models were limited in length to 100 mm long [16].

In this paper, the pre-existing model from [16] is developed, and it is proposed that the higher temperature under the electrode is due to the electrical current conducting through a smaller cross-sectional area, thus increasing the electrical resistance and associated power dissipated in this area. As the current flows from the edge of the entry electrode to the exit electrode at the edge of the sample, the cross-sectional conducting area increases. This is possible due to inter and intra ply contacts between carbon fibres. The electrode at the edge of the CFRP is the full thickness (4 mm) and width (40 mm) of the baton. Hence the electrical current is not as constrained in terms of cross-sectional conducting area as it is at the entry point. It is proposed that this can be modelled as the lumped resistance model in Fig. 3, and the total resistance is given by

$$R_{Tse} = R_{x1} + R_{x2} \qquad (3),$$

$$R_{x1} = \frac{l_e}{A_{x1}\sigma_x} \qquad (4),$$

$$R_{x2} = \frac{l_{ee}}{A_{x2}\sigma_x} \qquad (5),$$

where $R_{Tse}$ *(Ω)* is the total resistance of the pathway through the CFRP, $R_{x1}$ *(Ω)* is the resistance under the electrode in the $x$-direction, $l_e$ (m) is the length of the injection electrode in the $x$-direction, $A_{x1}$ *($m^2$)* is the cross-sectional conducting area in the $x$-direction, $\sigma_x$ is the electrical conductivity of the CFRP in the $x$-direction, $R_{x2}$ *(Ω)* is the resistive component between the edge of the electrode and the edge of the material in the x-direction, $l_{ee}$ *(m)* is the distance from the edge of the electrode to the edge of the CFRP with the electrode and $A_{x2}$ *($m^2$)* is the cross-sectional conducting area to the edge of the CFRP. Fig. 3 shows the lumped resistance model. The distances $l_e$ and $l_{ee}$ are defined in Fig. 4.

If the exit point from the CFRP is a second 10 x 10 mm square on the surface of the CFRP, as indicated in Fig. 4, then it is hypothesised that the electrical current will be constrained to the same cross-sectional conducting area at the exit point as the entry point, and hence the total resistance $R_{Tss}$ becomes

$$R_{Tss} = 2R_{x1} + R_{x2} \qquad (6),$$

where $l_{ee}$ in (6) is the distance between the two surface electrodes..

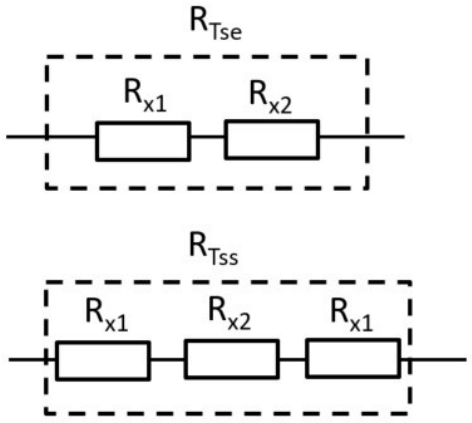


**Fig. 3: Proposed lumped reistance models, $R_{Tse}$ and $R_{Tss}$.**

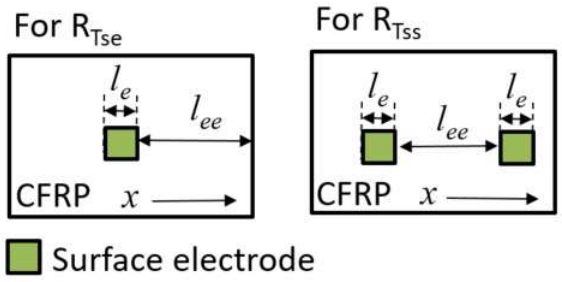


**Fig. 4: Definition of distances le and lee for calculation of $R_{Tse}$ and $R_{Tss}$**

*b. Experimental investigation of modelling hypothesis*

In order to investigate the electrical model proposed, it was first necessary to estimate the electrical conductivity in the infibre direction, $\sigma_x$, for the T800/HTC400 UD [0º] CFRP. The same method was used as described in [16], with samples of T800/HTC400 which were 10 mm wide, 4 mm (22 plies) thick and with length varied from 25 to 100 mm long. To minimise contact resistance, electrodes were prepared by sanding the surface of the CFRP with 320 grit sandpaper, and silver epoxy was then painted onto the prepared area. To measure the resistance, a copper foil was placed over the silver epoxy electrode and clamped in place using a vice (following the same methods as in [16]) to minimise contact resistance. Kelvin probes were used with an LCR meter to measure the electrical resistance. The electrical conductivity in the *x*-direction was measured to be 28 kS/m, with a contact resistance of 0.0137 Ω.

To investigate the electrical modelling hypothesis described in Section III a, three, 500 x 40 x 4 mm batons of CFRP were prepared with 5, 10 x 10 mm electrodes on the surface and an electrode along one 40 x 4 mm edge. For consistency and repeatability, electrodes were prepared using the same method as for estimating the electrical conductivity.

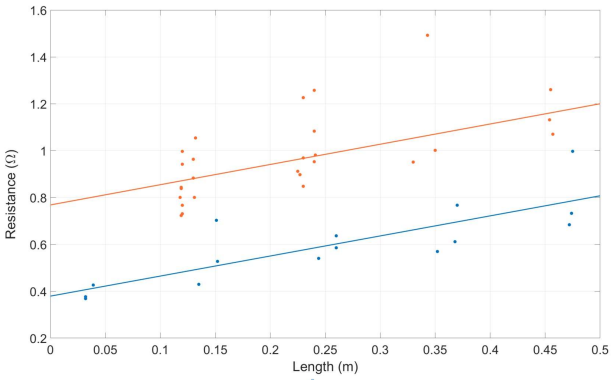


**Fig. 5: Variation of experimentally measured resitance, $R_{Tse}$ (blue dots) and $R_{Tss}$ (orange dots), with length, $l_x$, between entry and exit points, and the modelled relationship between $R_{Tse}$ and $l_x$ (blue line), and $R_{Tss}$ and $l_x$ (orange line).**

Two sets of results were collated. In one set the electrical resistance was measured between the surface electrodes and the edge of the CFRP. For the second set, the electrical resistance was measured between different pairs of electrodes on the surface of the CFRP batons. The results are plotted in Fig. 5, where the orange dots indicate the measured resistance between surface electrode and edge against the distance in the *x*-direction, $R_{Tse}$ *(Ω)*, and the blue dots indicate the measured resistance between surface electrodes, $R_{Tss}$ *(Ω)*, against distance in the *x*-direction.

From the experimental results, the relationship between $R_{Tse}$ and the distance, $l_x$ (m), is given by

$$R_{Tse} = 0.8564 l_x + 0.379 \quad (7),$$

where

$$l_x = l_e + l_{ee} \quad (8),$$

and the relationship between $R_{Tss}$ and $l_x$ is given by

$$R_{Tss} = 0.8361 l_x + 0.7682 \quad (9),$$

where

$$l_x = 2l_e + l_{ee} \quad (10).$$

The strong correlation in gradient between (7) and (9), and the fact that the constant in (9) is approximately twice that of the constant in (7) strongly supports the modelling hypothesis presented. Further work is needed to fully validate this model experimentally. The cross-sectional conducting area for the area under a 10 x 10 mm electrode is estimted using (4) to be ~ 9.42 x $10^{-7}$ $m^2$. The cross-sectional conducting area for the other section of conducting CFRP, is estimated using (5) to be ~4 x $10^{-5}$ $m^2$. For reference, the maximum cross-sectional area possible for the samples used is 1.6 x $10^{-4}$ $m^2$.

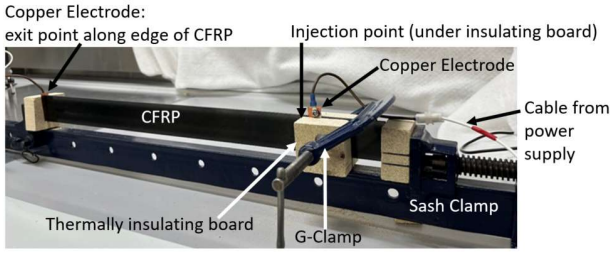


**Fig. 6: Experimental set up for injection of current through CFRP to capture electrical and thermal response.**

## IV. Temporal Thermal Response to Electrical Current Conduction

### a. *Aims and objectives*

While the resistance of the pathway taken by electrical current through CFRP influences the interaction of the CFRP with the electrical power system, it is also important to capture the temporal thermal response of the CFRP, as this provides further design criteria for the fault management system (e.g. speed of response to an electrical fault), and informs the relationship between electrical power dissipation and temperature.

By inspection of Fig.2, localised heating occurs along the conducting pathway of the CFRP. If this heating pushes the CFRP above glass transition temeprature of the resin, then this leads to degradation of the resin matrix. For the T800/HTC400 CFRP, $T_g$ is 272 ºC. The samples have not been post-cured, but the post-cure $T_g$ is 240 ºC. For these experiments, the temperature of 200 ºC was also noted as a critical temperature, as this is the glass transition temperture of other aerospace grade CFRP, such as IM7/8552 [ref epe].

The aim of these experiments was to estimate the power dissipated at the entry point of the CFRP, through an area of 10 x 10 mm, and correlate this to the time taken to reach the three threshold temperatures identified above. Previous work has not discriminated between the higher power dissipated where electrical current travels through a smaller cross-sectional area, and was limited to a total power dissipation of 90 W [8].

### b. *Experimental set up*

In order to capture the thermal response, 500 x 40 x 4 mm batons of UD [0º] T800/HTC400 were prepared with two electrodes: a 10 x 10 mm area was sanded 65 mm from the end of a 500 x 40 x 4 mm baton. Silver epoxy was not applied to the prepared area in order to replicate the effect of a chaffed cable forming a sold, electrical contact onto a panel of CFRP. The far end of the baton was prepared with a silver epoxy electrode, as for previous experiments and shown in Fig. 1. The electrodes were prepared as described earlier in the paper. Copper electrodes were held in place using a sash clamp (exit electrode) and G-clamp (entry electrode). Due to the high temperatures, the power supply cables were bolted to the copper foil electrodes, rather than soldered. The experimental set up is shown in Fig. 6. A constant voltage was applied across the electrodes from a power supply in each experiment. The voltage and current were captured using an NI cRIO, with temperature captured using a thermal camera, measuring the temperature at the edge of the injection point (edge of the insulating board). The time when the threshold temperatures of 272 ºC, 240 ºC and 200 ºC were reached was recorded.

### c. *Electrical and thermal response results*

The total power dissipated in the CFRP sample was calculated from the measured current conducted through, and voltage applied across, the CFRP. The power dissipated at the injection point was estimated using (2), with the resistance estimated from (7) of 0.379 Ω, and the measured current. For both cases, power dissipated was plotted against the time to reach threshold temperature, shown in Fig. 7 and Fig. 8 (shown as pale blue dots for time to reach 272 ºC, dark blue dots for time to reach 240 ºC and red dots for time to reach 200 ºC) In [8] it was proposed that the relationship between power dissipated and time to threshold temperature, $t_{threshold}$ *(s)* can be modelled using an equation of the form,

$$t_{threshold} = aP_i^b + c \qquad (11),$$

where $P_i$ *(W)* is the initial power dissipated, and *a, b* and *c* are constants. By applying (11) to the datasets in Figs. 7 and 8, the relationships between power dissipated and time to threshold temperatures were modelled, and are shown on Figs. 7 and 8 as solid lines. The co-efficients a, b and c from (11) are given in Table 1, for the total power dissipated in the full CFRP baton, and Table 2 for the power dissipated at the injection point into the CFRP.

## V. Discussions

### a. *Discussion of experimental results.*

Investigation of the electrical properties of UD [0 º ] CFRP for bigger panels has highlighted the impact of the constriction of the cross-sectional conducting area at the entry and exit points on the electrical resistance of the conducting pathway, and in particular on localised Joule heating. Further investigation is needed to fully correlate levels of power dissipated to temperatures reached, but results indicate that the time frame (for this particular lay-up) to reach threshold temperatures of 200 ºC and above are in the order of seconds, even for high levels of power dissipation. From an electrical protection perspective, this indicates that while electrical faults must be detected, but the speed of response can be relatively slow in the order of seconds.

It is interesting to note from the results presented in Figs. 7 and 8 and Table 1 and 2 , that the time to reach the threshold temperatures tend to similar values regardless of the initial power levels (“c” values in Tables 1 and 2). Further, while the time taken to reach the threshold temperature increases with temperature for the localised power dissipation at the injection

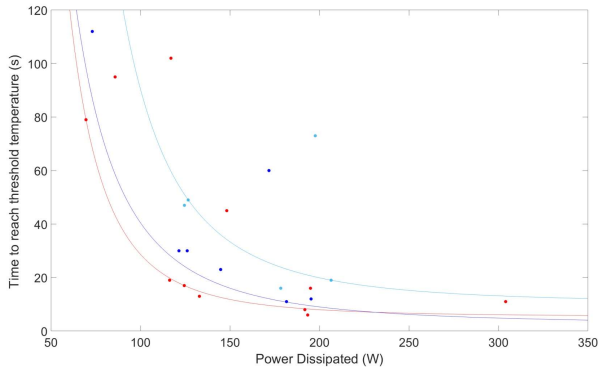


**Fig. 7: Total power dissipated in the CFRP against time to reach threshold temperature. Dots are experimentally measured time to reach 200 ºC (red), 240 ºC (dark blue), 272 ºC (pale blue). Solid lines are an estimation of the relationship between power dissipated and time to reach threshold temperature, 200 ºC (red), 240 ºC (dark blue), 272 ºC (pale blue), based on (11).**

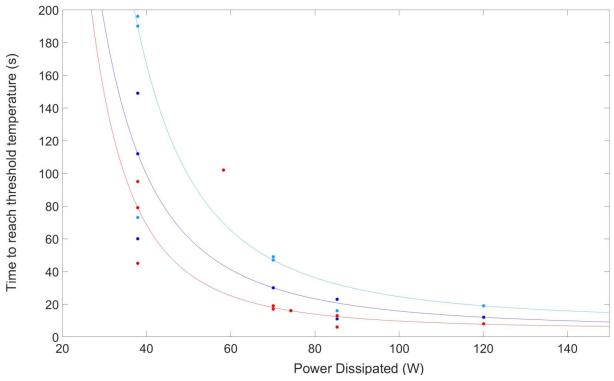


**Fig.8: Estimated power dissipated at entry point of CFRP against time to reach threshold temperatures. Dots are experimentally measured time to reach 200 ºC (red), 240 ºC (dark blue), 272 ºC (pale blue). Solid lines are an estimation of the relationship between power dissipated and time to reach threshold temperature, 200 ºC (red), 240 ºC (dark blue), 272 ºC (pale blue), based on (11).**

**Table 1: Co-efficients for equations describing relationship between power disspation and time to reach threshold temperatures for total power dissipated in CFRP.**

| Data Set | a | b | C |
|---|---|---|---|
| Time to reach 200 ºC | 5.2 x $10^7$ | -3.174 | 5.39 |
| Time to reach 240 ºC | 4.8 x $10^6$ | -2.553 | 2.553 |
| Time to reach 272 ºC | 1.2 x $10^8$ | -3.09 | 10.47 |

**Table 2: Co-efficients for equations describing relationship between power disspation and time to reach threshold temperatures for power dissipated at the injection point into CFRP.**

| Data Set | a | b | c |
|---|---|---|---|
| Time to reach 200 ºC | 2.1 x $10^6$ | -2.818 | 4.87 |
| Time to reach 240 ºC | 5.8 x $10^5$ | -2.364 | 4.995 |
| Time to reach 200 ºC | 1.96 x $10^6$ | -2.557 | 9.539 |

site (Fig. 8), this is not the case for the full power dissipated in the CFRP samples. It is acknowledged by the authors that more experimental data is needed to fully investigate these relationships. Improvements to the experimental method are needed to measure the temperature on the surface of the CFRP, and possibly within the CFRP.

### *b. Implications for integrated systems design*

The electrical model developed in Section III provides a basis for the design of methods for electrical bonding of CFRP to a current return network. Further, the method of electrically bonding to CFRP can be used as a method to control the electrical resistance added by a panel of CFRP to an electrical network, in a fault scenario. This may provide a pathway to tuning the CFRP to have a particular fault resistance, enabling resistance to be above or below threshold values for fault detection methods [8]. This will also influence the choice of grounding topology.

The impact of the size and location of the entry and exit points into, and out of a panel of CFRP, indicate the importance of understanding the fault manifestation process as this will directly influence both of these areas; first, in terms of size of contact area, the possible resulting high electrical resistance at that point; and second, in the location on a panel of CFRP where an electrical fault is likely to occur. If these two elements are known and combined with the basis of the model presented in this paper, then the impact of the CFRP on the fault response can be designed in parallel with the electrical power system.

## VI. CONCLUSIONS

This paper has presented an updated electrical model for UD [0º] CFRP, which has captured the influence of the physical size and location of electrical bonds to the CFRP. Over a longer distance, it appears despite the highly anisotropic nature of UD [0º] material, the electrical current will flow through a larger cross-sectional area resulting in a much lower electrical resistance than was predicted by previous published models.

Further work is needed to fully establish the relationship between electrical power dissipation in CFRP, variations in the level of power dissipation for different sections of a conducting pathway that have higher or lower, levels of electrical resistance and correlating these to temperatures reached. There is a need to develop appropriate experimental methods

to measure temperature both on the surface of the CFRP, but also within the CFRP. By continuing to develop the models presented in this paper, this will provide further basis for understanding how CFRP responds to electrical current, and what the thresholds are for failure. The authors will continue to work on these areas, first to progress towards the design of resilient, integrated systems and second, to support the development of appropriate industry standards.

## REFERENCES


1. B. Sarlioglu and C. T. Morris, "More electric aircraft: review, challenges and opportunities for commercial transport aircraft". *IEEE Transactions on Transportation Electrification,* Vol. 1, No. 1, Pages 54-64, 2015
2. "Boeing 787 from the ground up", Aero Magazine, Boeing, qtr_4, Chapter 4, 2006, [online], Available: https://www.boeing.com/commercial/aeromagazine/srticles/qtr_04_06/article_04_2.html
3. SAE Aerospace, "Aerospace Recommended Practice 1870: Aerospace systems electrical bonding and grounding for electromagnetic compatibility and safety", SAE International Group 2012.
4. J. Chua, "Supplement to m6.11/M7.07 EWI: Bonding and grounding network for composite structure aircraft", Temasek Polytechnic, 2018.
5. U. Schwark and C. Pichavant, "WRC-15 Agenda Item 1.17 – Industry's Motivation", EC-CEPT Workshop on WRC-15, 2013.
6. J. Benzaquen, J. He and B. Mirafzal, "Toward more electric powertrains in aircraft: technical challenges and advancements", *CES Trans. on Electrical Machines and Systems,* Vol. 5, No. 3, 2021.
7. C.E.Jones et al, "A route to sustainable aviation: a roadmap for the realization of aircraft components with electrical and structural multifunctionality", *IEEE Transactions on. Transportation Electrification*, Vol. 7, Issue 4, 2021.
8. C.E. Jones et al, "Electrical and thermal effects of fault currents in aircraft electrical power systems with composite aerostructures", *IEEE Transactions on. Transportation Electrification*, Vol. 4, No. 3, 2018.
9. A. Piche et al, "Dynamic electrical behaviour of a composite material during a short circuit", *10th International Symposium on Electromagnetic* Compatibility, 2011.
10. J. B. Khan et al, "Experimental electrical characterisation of carbon fibre composites for use in future aircraft applications", *IET Science, Measurement and Technology*, 2019.
11. "T800H Intermediate modulus carbon fiber", Toray, 2018, online, available:www.toraycma.com
12. "HTC400 Epoxy Component Prepreg", SHD Composites, 2022, online, available:www.shdcomposites.com/admin/resources/htc400-tds-1.pdf
13. K. Dong, B. Gu, and B. Sun, "Comparisons of thermal conductive behaviors of epoxy resin in unidirectional composite materials," *Journal of Therm. Anal. Calorim*., 2016
14. D.P.H. Hasselman and L.F. Johnson, "Effective thermal conductivity of composites with interfacial thermal barrier resistance", *J. Composite Materials*, 1987.
15. F. D. Senghor, G. Wasselynck and H.K. Bui, "Electrical conductivity tensor modelling of stratified woven-fabric carbon fiber reinforced polymer composite materials", *IEEE Transactions on Magnetics*, Vol. 53, No. 6, 2017.
16. C. E. Jones et al, "Electrical model of carbon fibre reinforced polymers for the development of electrical protection systems for more-electric aircraft", 18th European Conference on Power Electronics and Applications, 2016.
17. B.G. Moffat, "Failure mechanisms of legacy aircraft wiring and interconnects", *IEEE Transactions on Dielectrics and Electrical Insulation,* Vol. 15, Issue 3, 2008.
18. M. Teroede, H. Wattar and D. Schulz, "Phase balancing for aircraft electrical distribution systems", *IEEE Transactions on Aerospace and Electronic Systems*, vol. 51, no. 3, 2015.
19. Federal Aviation Administration, "Advisory circular 43.13 -1B: Acceptable methods, techniques and practices – aircraft inspection and repair", U.S. Department of Transportation, 1998.